Boundary-Layer Meteorology (2019) 173:99–113
https://doi.org/10.1007/s10546-019-00453-4

RESEARCH ARTICLE

Effects of Path Averaging in a Sonic Anemometer on the Estimation of Turbulence-Kinetic-Energy Dissipation Rates

Livia S. Freire[1] · **Nelson L. Dias**[2] · **Marcelo Chamecki**[3]

Received: 14 November 2018 / Accepted: 29 April 2019 / Published online: 4 June 2019

Abstract
The turbulence-kinetic-energy dissipation rate is a fundamental property in turbulent flows, but its direct measurement in the atmospheric surface layer is still a challenge. Indirect estimates are often obtained from inertial-subrange laws using turbulence statistics of the longitudinal velocity component. In this study, synthetic turbulence data are used to investigate the impact of path-averaging effects present in sonic anemometer data on the inertial subrange of the second-order structure function. Path averaging reduces the energy levels in the second-order structure function, creating a negative bias in the estimates of the dissipation rate. The effect is dependent on the path-averaging transfer function, mean wind speed and path length. A simple correction for the bias on the basis of existing transfer functions is applied and tested with data obtained from two separate sonic anemometers. Compared to the spectrum, the second-order structure function after the correction becomes the optimum statistical measure for indirect estimation of the dissipation rate, due to its lower random error and insensitivity to aliasing effects.

Keywords Correction · Energy spectrum · Path averaging · Second-order structure function · Sonic anemometer

✉ Livia S. Freire
liviagrion@gmail.com

Nelson L. Dias
nelsonluisdias@gmail.com

Marcelo Chamecki
chamecki@ucla.edu

[1] Graduate Program in Environmental Engineering, Federal University of Paraná, Curitiba, PR, Brazil

[2] Department of Environmental Engineering, Federal University of Paraná, Curitiba, PR, Brazil

[3] Department of Atmospheric and Oceanic Sciences, University of California, Los Angeles, CA, USA

1 Introduction

The mean dissipation rate of turbulence kinetic energy (hereafter TKE dissipation rate or ε) is a fundamental property of turbulent flows, as it corresponds to the rate of energy transfer across the energy cascade of a stationary flow and can be used to define length and time scales characteristic of the structure of turbulence (Pope 2000; Davidson 2004). In the atmosphere, it has been used for different purposes, such as the inertial dissipation method for flux estimation (Fairall and Larsen 1986; Hsieh and Katul 1997; Henjes 1998), to evaluate anisotropy (Warhaft 2000; Chamecki and Dias 2004), for the evaluation of scalar similarity (Cancelli et al. 2012), to characterize wind-turbine wakes (Smalikho et al. 2013), to estimate Lagrangian dispersion of passive scalars and particles (Poggi et al. 2006; Wilson 2000), and for construction of a reduced TKE phase space used to characterize disturbed surface-layer flows (Chamecki et al. 2018). Furthermore, recent studies have shown that the length scale $\ell_\varepsilon = u_*/\varepsilon$ (where u_* is friction velocity) is the correct scale for the non-dimensionalization of some statistics obtained in the atmospheric surface layer (ASL) (Davidson and Krogstad 2014; Pan and Chamecki 2016; Chamecki et al. 2017). However, the lack of direct estimates of ε in the atmosphere still poses a limitation in turbulence studies. To overcome this issue, indirect estimates are usually obtained from the inertial-subrange laws derived by Kolmogorov for the velocity spectrum and structure function of the longitudinal velocity fluctuations. This method is sensitive to measurement error, in addition to the error in the empirical Kolmogorov constants in the case of the spectrum and the second-order structure function (Chamecki and Dias 2004). Although the third-order structure function does have an analytical constant (4/5), second-order structure functions usually display a clearer inertial subrange (Albertson et al. 1997), so that they remain more popular in the atmospheric turbulence community.

In studies of the ASL, discrepancies in the TKE dissipation rate values obtained from different inertial-subrange statistics have been observed. For example, Chamecki and Dias (2004) obtained values estimated from second- and third-order structure functions that are, on average, 10 and 30% lower than estimates using the spectrum, respectively. Albertson et al. (1997) and Chamecki et al. (2017) obtained estimates from the third-order structure function that are respectively 20% and 30% lower than the estimates from their second-order counterparts. Such systematic discrepancies are often justified by the errors in the empirical constants of the second-order statistics, or to deviations from the local isotropy hypothesis in the ASL.

When velocity fluctuations are measured with a sonic anemometer, path averaging can affect determination of the spectrum and the structure functions to different degrees. In the ASL, the range of scales in the inertial subrange captured by a sonic anemometer is not large enough to avoid these effects. Despite this issue being well known, its impact on the estimates of TKE dissipation rates usually are not taken into account.

In the present study, we generate synthetic data that mimic longitudinal velocity time series with an imposed TKE dissipation rate, second-order statistics and random errors, which are used to compare errors and biases present in ε estimates from the spectrum and the second-order structure function, before and after the introduction of path-averaging effects. A correction for the path-averaging bias in the second-order structure function is proposed and then tested with actual data from two separate sonic anemometers.

Despite its importance, the third-order structure function is not used here, as it has a less distinct inertial subrange than its second-order counterpart and is more affected by anisotropy (Chamecki and Dias 2004). In addition, synthetic models that mimic third-order

turbulence statistics have a large uncertainty in the dissipation rate, contaminating error and bias analyses such as those performed here. Therefore, we restrict our study to second-order statistics.

2 Theory

The one-dimensional, longitudinal velocity spectrum $E_{11}(k_1)$ can be defined as twice the Fourier transform of the longitudinal correlation function $R_{11}(r_1) = \langle u_1(x_1)u_1(x_1 + r_1)\rangle$, i.e.,

$$E_{11}(k_1) \equiv \frac{2}{\pi}\int_0^\infty R_{11}(r_1)\cos(k_1 r_1)dr_1, \tag{1}$$

where u_1 is the longitudinal velocity fluctuation, x_1 is the longitudinal spatial coordinate, r_1 is the longitudinal spatial separation, k_1 is the longitudinal wavenumber and $\langle\ \rangle$ represents the ensemble average. In isotropic turbulence, statistics are invariant under reflections and rotations and R_{11} can then be redefined as $u^2 f(r_1)$, where $u^2 = \langle u_1^2\rangle = \langle u_2^2\rangle = \langle u_3^2\rangle$ (indices 2 and 3 are used for the spanwise and vertical directions, respectively) can be used to define a velocity scale and $f(r_1)$ is a longitudinal dimensionless correlation function (Davidson 2004, p. 89). Note that in this case $\int_0^\infty E_{11}(k_1)dk_1 = u^2$.

The nth-order, longitudinal structure function is

$$\Delta u^n(r_1) \equiv \langle [u_1(x_1 + r_1) - u_1(x_1)]^n\rangle, \tag{2}$$

which for $n = 2$ can also be redefined as a function of $f(r_1)$, as $\Delta u^2(r_1) = 2u^2[1 - f(r_1)]$, leading to a relation with the spectrum in the form (Pope 2000, p. 226)

$$\Delta u^2(r_1) = 2\int_0^\infty E_{11}(k_1)\left[1 - \cos(k_1 r_1)\right]dk_1. \tag{3}$$

This relation highlights the fact that the spectrum and the second-order structure function are two different ways of representing the underlying spatial structure of the velocity field.

For the special case of the inertial subrange, the spectrum and structure function laws obtained by Kolmogorov provide a suitable way to estimate ε in situations where it cannot be measured directly. For $1/L \ll k_1 \ll 1/\eta$ and $\eta \ll r_1 \ll L$ (where L and η are the integral and dissipation length scales, respectively)

$$E_{11}(k_1) = \alpha\varepsilon^{2/3}k_1^{-5/3}, \tag{4}$$

and

$$\Delta u^2(r_1) = \beta\varepsilon^{2/3}r_1^{2/3}. \tag{5}$$

From (3), in the idealized case of an infinitely large inertial subrange, a direct relation between the constants α and β can be obtained. The conditions that guarantee a good approximation for real turbulence data were presented by Webb (1964) and Monin and Yaglom (1981, p. 356): if $1/k_{1,\max} \ll r_{1,\min} < r_{1,\max} \ll 1/k_{1,\min}$ (where $k_{1,\min}, k_{1,\max}, r_{1,\min}$ and $r_{1,\max}$ set the boundaries of the inertial subrange) the well-known relation $\beta \approx 4\alpha$ (Pope 2000, p. 232) is valid. The reduced size of the structure function's inertial subrange

compared to the sprectum is a consequence of the "contamination" in the second-order structure function of the production and dissipation ranges of the spectrum, which have lower energy compared to the Kolmogorov law for the same wavenumber. This requirement for $\beta \approx 4\alpha$ is usually met for large Reynolds-number flows, such as those in the ASL. However, as will be seen in Sect. 4, path averaging introduced by the sonic anemometer limits the practical width of the inertial subrange, affecting this relation. Instead of correcting the constants to include path-averaging effects, we propose a correction to recover the condition in which $\beta \approx 4\alpha$ is valid.

3 Data and the Path-Averaging Effect

3.1 Synthetic Data

To investigate the effects of path averaging in the estimation of ε from inertial-subrange laws, we use a synthetic model that mimics measurements of the longitudinal velocity component from sonic anemometers with a known value of ε. Time series of a synthetic velocity u_1^s were generated using the spectral method developed by Shinozuka and Deodatis (1991). The velocity time series is given by

$$u_1^s(t) = \mathrm{Re}\left\{ \mathrm{FFT}\left\{ [S(f)\Delta f]^{1/2} \sqrt{2} \mathrm{e}^{i\phi(f)} \right\} \right\}, \tag{6}$$

where Re{} denotes the real part of a complex number, FFT{} is the fast Fourier transform, $S(f)$ is the desired spectral density of $u_1^s(t)$ as a function of frequency f, Δf is the frequency increment and $\phi(f)$ is a random variable uniformly distributed between 0 and 2π, used to obtain independent random phase angles that create the velocity fluctuations in the time domain. As discussed by Shinozuka and Deodatis (1991), the distribution of $u_1^s(t)$ tends to Gaussian on the limit of infinite phases being summed; however this is not valid for spectral slopes steeper than f^{-1} (Jiménez 1998), which is the case in this study, as described below.

Equation 6 provides a time series with spectral density corresponding exactly to the chosen model for $S(f)$, except for small errors due to numeric truncation. To mimic the random errors inherent in real sonic-anemometer data, we define $S(f) = F_{11}(f) + \sigma(f)y$, where $F_{11}(f) = E_{11}(k_1)2\pi/U$ is the spectrum in the frequency domain, U is the mean wind speed, $\sigma(f)$ is the standard deviation of real spectra and y is a random variable. In addition, assuming a quasi-normal hypothesis, the standard deviation of the spectrum is equal to its mean value (Bendat and Piersol 2010; Dias 2017), which gives $S(f) = F_{11}(f)(1 + y)$ with $2(y + 1)$ following a chi-square distribution with two degrees of freedom (since the spectrum corresponds to the square of a normally-distributed random variable). Note that the expected value and variance of y are zero and one, respectively.

Because we are focused on the inertial subrange, $F_{11}(f)$ is chosen to correspond to the Kolmogorov law (given by Eq. 4 multiplied by the factor $2\pi/U$) in the entire frequency range simulated ($5.56 \times 10^{-4} \leq f \leq 2$ kHz). This choice makes the distribution of $u_1^s(t)$ slightly sub-Gaussian (Jiménez 1998), with a kurtosis ≈ 2.8. Aliasing effects present in measurements were introduced by resampling $u_1^s(t)$ at a frequency of 20 Hz. Path averaging was simulated by using

$$S(f) = F_{11}(f)(1 + y)H_u(fp\pi/U), \tag{7}$$

where $H_u(fp\pi/U)$ is a transfer function obtained from the ratio of the path-averaged to the true one-dimensional, longitudinal velocity spectrum (Kaimal et al. 1968; Horst and Oncley 2006). For the synthetic data we test the simplest case where a single path length in the longitudinal direction is present, corresponding to $H_u(fp\pi/U) = \mathrm{sinc}^2(fp\pi/U)$ with a path length $p = 0.15$ m ($\mathrm{sinc}(x) = \sin(x)/x$).

Apart from the aforementioned random error introduced to mimic measurement errors, this model does not present any variability in the imposed value of ϵ. This was the crucial reason in the choice of this simple model approach over other synthetic models available in the literature (e.g. the model proposed by Juneja et al. 1994). The final values of $u_1^s(t)$ at 20 Hz are equivalent to a series obtained from a sonic anemometer, where both aliasing and path-averaging effects are present in the spectrum. The second-order structure function obtained from this series also presents path-averaging effects, as will be discussed in Sect. 4.

In order to test a path-averaging correction that can be applied to field data, the spectrum obtained from $u_1^s(t)$ is divided by $H_u(fp\pi/U)$ (recovering the spectrum without path averaging), a new velocity series is obtained by performing an inverse FFT to the corrected spectrum, and from it a corrected second-order structure function can be estimated. Note that, although there are methods available to reduce the aliasing effect from the spectrum (e.g. Gobbi et al. 2006), they should not be applied if the goal is to correct the second-order structure function, since the aliased energy is real and should be present in $\langle \Delta u^2 \rangle$.

Despite the fact that the synthetic data do not have the super-Gaussian nature of small-scale turbulence, this difference is not expected to affect the analysis presented herein. First, the relationship between the spectrum and second-order structure function (3) does not depend on higher-order statistics of the velocity fluctuations. Second, the Kolmogorov law for the inertial subrange and, consequently, the estimation of ϵ from the spectrum and second-order structure function are also independent of higher-order statistics. And finally, there is no assumption of Gaussianity on the transfer-function estimations and consequently on the correction proposed here. Therefore, for the purpose of investigating the path-averaging effects (and its correction) on the spectrum and second-order structure function, this synthetic model can be considered appropriate.

To simplify the calculations, results presented in Sect. 4 were obtained with $U = 2\pi\,\mathrm{m\,s^{-1}}$ (so wavenumber and frequencies are equivalent) and an imposed dissipation rate equal to $1\,\mathrm{m^2\,s^{-3}}$. All calculations were performed for a 30–min time series. Dissipation rates were estimated by fitting the Kolmogorov law to the compensated spectrum and structure function in the ranges $1 \leq f \leq 5$ Hz and $0.5 \leq r_1 \leq 1$ m, respectively. No smoothing of the spectrum was performed, as it did not produce any significant change in the results.

3.2 Field Data

Data collected at the Rio Verde dam in Araucária county, state of Paraná, Brazil (25°31′30″S, 49°31′30″W) are used to test the correction proposed for the second-order structure function. Data were obtained simultaneously using a 81000 Ultrasonic anemometer from Young (Traverse City, Michigan, USA) and an IRGASON gas analyzer and sonic anemometer from Campbell Scientific (Logan, Utah, USA), both at 20 Hz, from 25 September to 4 October 2017. Sensors were installed a few meters above the water surface, at the border of the dam, facing the preferential mean wind direction. Data were separated into 30-min blocks starting at midnight local time, and post processing and data selection

were performed following Zahn et al. (2016). A final number of 59 blocks for each anemometer was obtained.

Estimations of TKE dissipation rate from the spectrum and second-order structure function were obtained before and after the application of path-averaging correction. As in the synthetic data, the correction comprised four steps: (i) estimating the energy spectrum; (ii) estimating a corrected spectrum by dividing it by the transfer function H_u; (iii) performing an inverse FFT to create a time series whose spectrum corresponds to the corrected spectrum; and (iv) estimating a corrected second-order structure function from it. Note that this time series created by the inverse FFT is *not* a corrected time series, but rather a time series whose spectrum is equal to the corrected spectrum. Note also that this correction aims to "recover" the energy lost due to path averaging on the spectrum, and to transfer this information to the second-order structure function with the sole purpose of estimating the dissipation rate. Because no correction is applied to higher-order statistics (the third-order structure function, for example), other information extracted from the corrected data (such as skewness and kurtosis of velocity increments) may not be correct.

Based on the geometry of the sensors, the transfer functions calculated by Horst and Oncley (2006) for the Solent R3 and CSAT3 anemometers were used for the Young and Campbell anemometers, respectively. Note that there is a 30º rotation angle about the sonic's vertical axis difference between the IRGASON and CSAT3 instruments, which can be taken into account by adding 30º to the wind direction term in the original equation. The same frequency and streamwise distance ranges used for the synthetic case were used to estimate dissipation rates from the field data by performing a fitting of the Kolmogorov law to the compensated spectra and second-order structure functions.

4 Results

4.1 Synthetic Turbulence

Figure 1a shows an example of a spectrum generated by the synthetic model. The random error of the model, reflected in the level of scatter around the Kolmogorov law (imposed as the mean value), is similar to the error obtained in real turbulence data (see Fig. 4 for an example). The aliasing effect when the data frequency is reduced from 2 kHz to 20 Hz is clearly observed in the mean spectrum (also shown in Fig. 1a). As expected, at this stage the corresponding second-order structure function has a well-defined inertial subrange (Fig. 1b).

The path-averaging effect introduced in the model is shown in Fig. 1c, which counterbalances most of the aliasing in the 20-Hz spectrum, significantly reducing the region where the spectrum differs from the Kolmogorov law. The second-order structure function, on the other hand, is seriously affected by path averaging; a consistent reduction in its value can be observed in the region corresponding to the inertial subrange, being larger for lower values of r_1 (see Fig. 1d). Note that the impact is still significant for values of r_1 much larger than the path length, due to the integral nature of the structure function (3). This situation is equivalent to the estimation of the TKE dissipation rate in the ASL from sonic anemometer data. Note that, at this stage, there is an over/underestimation of the levels of the spectrum/structure function in the inertial subrange, which directly impacts the estimation of ε.

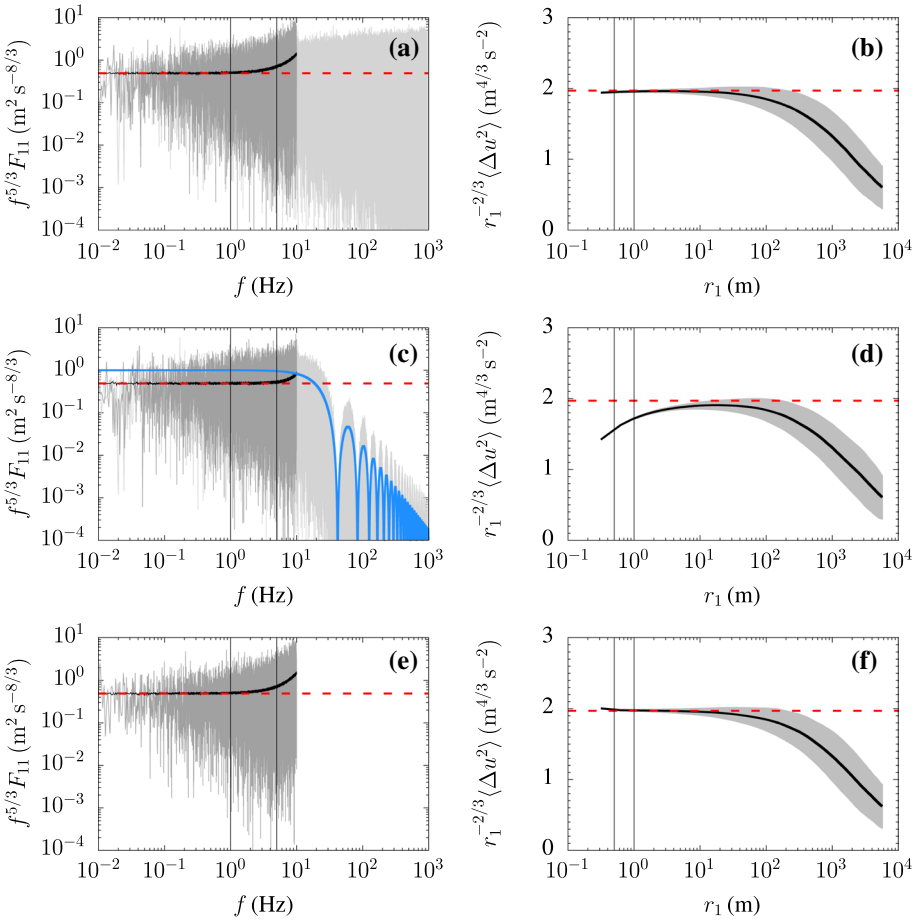

Fig. 1 Synthetic compensated spectra (left panels) and second-order structure functions (right panels) without path averaging (**a**–**b**), with path averaging (**c**–**d**) and with path averaging and correction (**e**–**f**). Full data (up to 2 kHz) in light-grey, resampled at 20 Hz in dark-grey, average of 1000 tests in black (**a**, **c**, **e**); path-averaging equation in blue (**c**); average of 1000 tests in black, average ± standard deviation in grey (**b**, **d**, **f**). In all plots, red line corresponds to the Kolmogorov inertial subrange law and vertical lines delimit the range used to estimate ε

The correction of the path-averaging effect in the 20-Hz data is effective in recovering the original result in both the spectrum and the second-order structure function (Fig. 1e, f respectively). Since aliasing affects the inertial subrange of the spectrum, this result indicates that the best approximation to Kolmogorov's prediction is the structure function after the path-averaging correction. In this case the range of r_1 values at which the dissipation range can be estimated is increased, reducing both the bias and the error of the estimate.

Figure 2 summarizes the distribution of values of ε obtained from each type of estimation, using 1000 runs of synthetic turbulence (exact values of mean and standard deviation are presented in Table 1). Without path averaging (dotted lines), the estimates from the spectrum have a positive bias of 30% due to aliasing, whereas estimates from the second-order structure function have a negative bias of less than 1%. With path averaging (dashed lines), the negative bias of the structure function estimates reaches 22%, whereas the

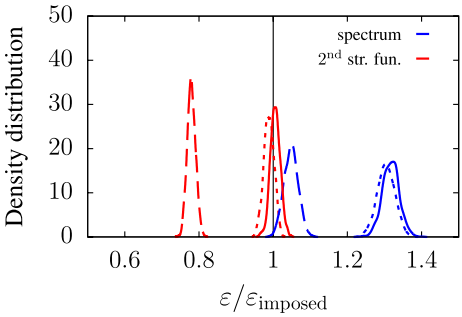

Fig. 2 Probability density functions obtained from 1000 realizations of synthetic turbulence resampled at 20 Hz, without path averaging (dotted lines), with path averaging (dashed lines) and with path averaging and correction (solid lines)

Table 1 Values of mean ± standard deviation of $\varepsilon/\varepsilon_{\text{imposed}}$ estimated from synthetic data

	Spectrum	2nd-order structure function
Without path averaging	1.30 ± 0.024	0.99 ± 0.014
With path averaging	1.05 ± 0.019	0.78 ± 0.011
Corrected path averaging	1.32 ± 0.023	1.01 ± 0.013

positive bias of the spectrum is greatly reduced. Note that in reality the balancing effect between aliasing and path averaging in the spectrum will vary from run to run (among other factors, H_u is a function of U, for example), which can generate different biases for the spectrum estimate depending on the data. This is another reason that makes the structure-function estimation more reliable. After correction (solid lines), estimates from the structure function have a small positive bias of less than 1%, whereas spectral estimates return to their original values. This result, combined with its smaller standard deviation, makes the corrected structure function the best approach for estimating ε.

It is important to point out that the exact values of bias are a function of the f and r_1 intervals used to estimate ε from each function: in the present exercise, we chose typical values used in the literature. Also, errors in spectrum estimates can be reduced by averaging over a longer inertial subrange interval; we used a range that is similar to what is available in experimental data. The error in the estimation using the second-order structure function is less dependent on the size of the r_1 interval used, but it is lower for smaller r_1 values (see standard deviation in Fig. 1). Note that because the random errors introduced in the synthetic model are similar to the ones present in real spectrum, these values of standard deviation are probably a good estimate of the random errors present in real ε estimates from sonic anemometer data. Finally, the effects of path averaging on ε estimates are smaller the lower the path length of the sensor, as expected (for example, the second-order structure bias without correction is reduced to -11% for $p = 0.05$ m; not shown). Despite these variations in exact values of errors and biases, the overall conclusion that the smaller error and bias is obtained from the corrected second-order structure function remains solid.

4.2 Field Data

Now we test the effect of the path-averaging correction on real turbulence data from two separate sonic anemometers. Because there is no measurement of the real dissipation rate,

there is no way to know exactly how much error and bias are present in each estimate of ε. However, based on the results obtained from the synthetic data, we expect that the estimate from the corrected second-order structure function is the most reliable one.

Figure 3 presents examples of transfer functions calculated by Horst and Oncley (2006) for each anemometer. Note that, while the measurement frequency is fixed (it goes from 5.56×10^{-4} to 20 Hz), the transfer function is affected by the mean longitudinal velocity component. Therefore, each 30-min run will have a different path-averaging effect. For values of wind speed $\gtrsim 10\,\mathrm{m\,s^{-1}}$ and measurement frequency of 20 Hz, the path-averaging effect becomes increasingly smaller. The final impact of the correction on the dissipation rate, however, must be assessed for each specific case (sonic anemometer geometry and measurement frequency, for example).

Figure 4 presents an example of measured spectrum and second-order structure function, for the run obtained on 25 September 2017 at 2230 LT (local time = UTC −3h) by each anemometer, before and after the path-averaging correction. Note that, as found with the synthetic data, the correction increases the overestimation of spectral densities due to aliasing, and it fixes the inertial subrange of the second-order structure function. For the Young anemometer, the final result is very close to the Kolmogorov law; for the Campbell anemometer, there is some underestimation left, possibly due to other sensor effects (see the average of all runs in Fig. 5).

Dissipation rates estimated from spectrum and second-order structure function before and after correction for all runs are presented in Fig. 6. On average, dissipation increased by 31 and 26% for spectrum and structure estimates, respectively, for the Young data, and by 19% in both estimates for the Campbell data. Considering, from the synthetic data, that the corrected second-order structure function provides the best estimate, the uncorrected spectrum has an overestimation of $\approx 20\%$ and the corrected spectrum has an overestimation of $\approx 50\%$, on average.

For the Young anemometer and the values of wind speed measured at the Rio Verde dam, there is a tendency of decreasing dissipation rate error due to path averaging with increase of wind speed (Fig. 7a), as expected from the transfer function behaviour (see Fig. 3). In the case of the Campbell anemometer, on the other hand, the error is approximately constant for wind speeds between 1 and $6\,\mathrm{m\,s^{-1}}$ (Fig. 7a), likely due to the pronounced secondary peak in the transfer function at $k_1 p \approx 9$. Although at high wind speeds

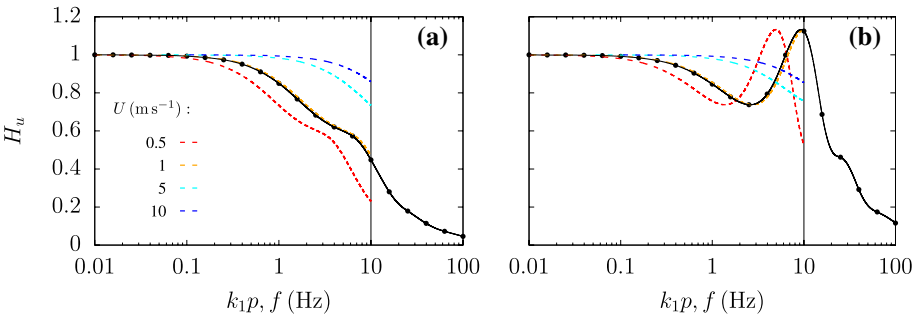

Fig. 3 Transfer functions (H_u) for **a** Young and **b** Campbell sonic anemometers. Black solid lines with dots correspond to the values estimated by Horst and Oncley (2006), as a function of the wavenumber normalized by the path length ($k_1 p$). Dashed lines correspond to H_u as a function of the frequency (f), for different values of mean wind speed (U). Vertical line corresponds to the Nyquist frequency of the measurements presented here

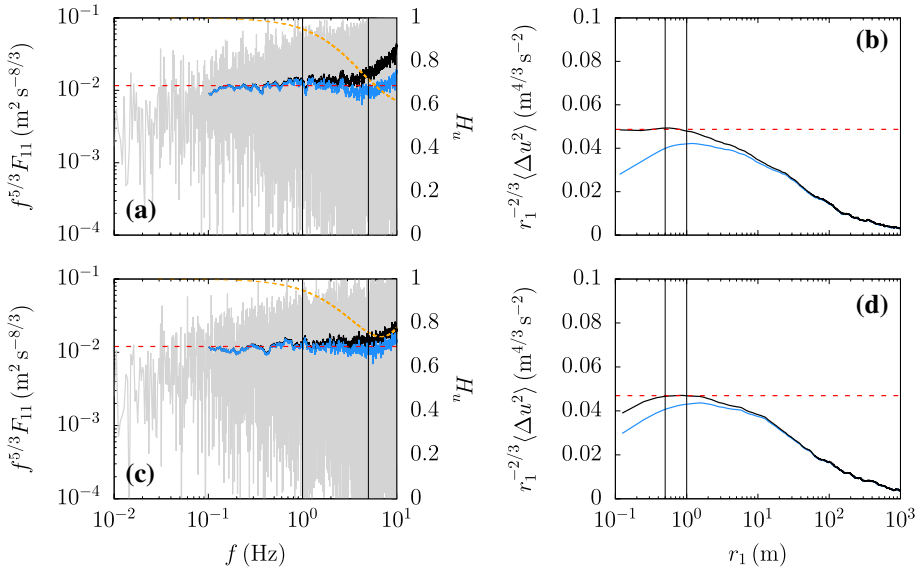

Fig. 4 Compensated longitudinal spectrum (left panels) and second-order structure function (right panels) measured by the Young anemometer (upper panels) and Campbell anemometers (lower panels). Light-grey is the original spectrum, black and blue lines are the smoothed spectra (moving average with a 100-point window). For both statistics, the blue line is before the path-averaging correction, and the black line is after. The orange line is the transfer function used. The red line is the slope of the Kolmogorov law. Vertical lines delimit the interval used for ϵ estimation. Measurements were made on 25 September 2017 at 2230 LT

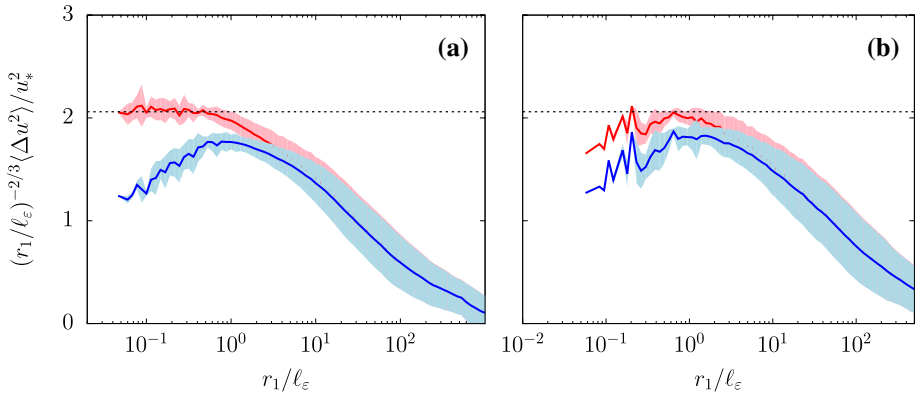

Fig. 5 Mean values (solid lines) ± one standard deviation (shaded area) of the normalized compensated second-order structure function before (blue) and after (red) path-averaging correction, for the Young (**a**) and Campbell (**b**) anemometers. Horizontal line is a fit for the mean inertial subrange of the Young anemometer. Values normalized by the dissipation length scale $\ell_\varepsilon = u_*^3/\epsilon$ and the friction velocity u_* (values of ϵ estimated after correction were used)

it is likely that the correction becomes increasingly less important, for all values observed in the Rio Verde experiment the correction increased the value of the estimated dissipation rate.

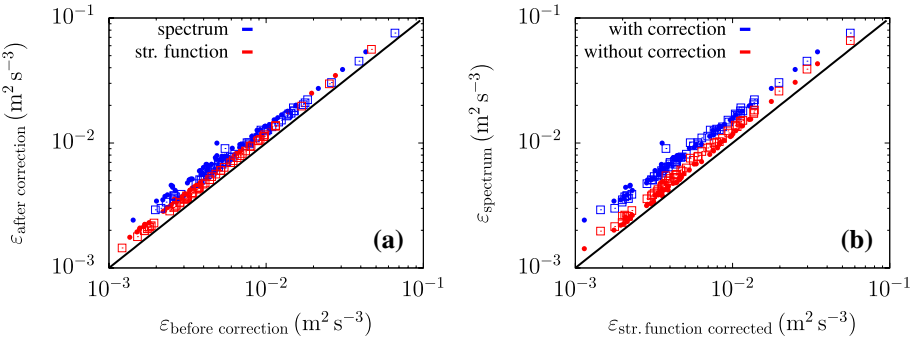

Fig. 6 **a** Comparison between dissipation rates estimated from spectrum (blue) and second-order structure function (red) before and after correction, using Young (dots) and Campbell (squares) anemometers. On average, spectrum estimates increased by 31% (Young) and 19% (Campbell) after correction, whereas second-order structure function estimates increased 26% (Young) and 19% (Campbell). **b** Dissipation rates estimated from uncorrected (red) and corrected (blue) spectrum, compared with corrected second-order structure function estimates, using Young (dots) and Campbell (squares) anemometers. On average, spectrum estimates are overestimated by 20% (Young) and 24% (Campbell) when uncorrected, and by 58% (Young) and 48% (Campbell) when corrected

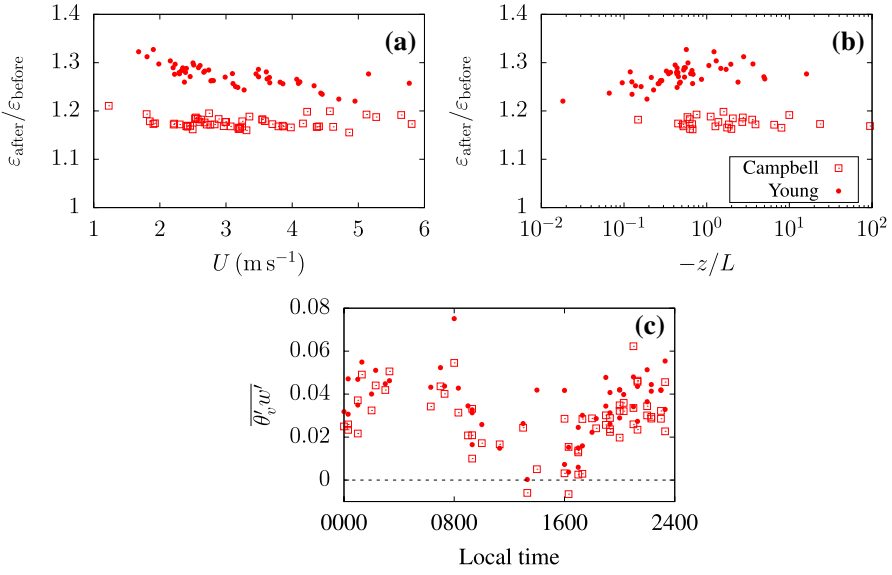

Fig. 7 Ratio between the dissipation rates estimated from the second-order structure function after and before correction as a function of, **a** mean wind speed, and **b** atmospheric stability, using Young (dots) and Campbell (squares) anemometers. **c** Sensible heat flux as a function of local time

When the inertial subrange has a $-5/3$ slope, the relationship between atmospheric stability and the correction should not be relevant, as stability impacts the spectrum mostly in the production range (Kaimal et al. 1972). As expected, the correction will not be valid for cases when the Kolmogorov law fail to represent the inertial subrange, as observed in very stable cases, for example (Lumley 1964). For the Rio Verde data, the dissipation rate error

vary with atmospheric stability with the same tendency observed for wind speed (Fig. 7b), i.e., increase of error for increasing instability in the case of Young anemometer (unstable cases tend to be related to lower wind speeds) and a constant error with stability for the case of Campbell anemometer. Here the atmospheric stability is represented by the stability parameter z / L, where $z \approx 4$ m is the distance from the water surface and L is the Obukhov length. Note that all data presented here display a positive heat flux (and consequently neutral and unstable conditions) in spite of the measurement local time (Fig. 7c). There are two measurements of very small negative heat flux by the Campbell anemometer, but their stability could not be defined because the momentum flux for these data is positive, evidencing rather exceptional conditions; for this reason they are not presented in Fig. 7b (the differences between the anemometers are out of the scope of the present study).

5 A Note on the CSAT3 Sonic Anemometer Manufactured by Campbell Scientific

In the field experiment described in Sect. 3.2, data from a CSAT3 sonic anemometer by Campbell Scientific were also collected; therefore, a similar correction as performed in the IRGASON data could also be tested. However, the second-order structure function from CSAT3 sonics presents a distinct feature that cannot be explained by the path-averaging effect, or any other effect known to the authors. In the lowest values of the time lag τ, within the inertial subrange, there is an increase in values of $\langle \Delta u^2 \rangle$ compared to the Kolmogorov law, instead of the decrease observed due to path averaging (Fig. 8). This feature seems to be characteristic of the CSAT3 model (and not of a specific sensor), as a similar behaviour can be observed in data measured by different sensors in different field experiments (see for example data from the AHATS (Salesky and Chamecki 2012) and the GoAmazon (Fuentes et al. 2016) experiments). This feature also does not seem to be related to atmospheric stability (these examples were arbitrarily chosen from each dataset). None of the known sonic anemometer effects discussed in the literature (e.g. flow distortion by transducer shadowing, (Horst et al. 2015)) is the cause of this behaviour; an investigation is left for future studies.

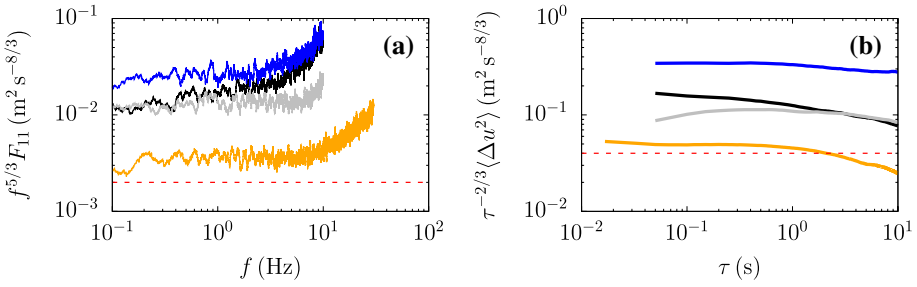

Fig. 8 Compensated longitudinal **a** spectrum and **b** second-order structure function measured by CSAT3 sonic anemometer from Rio Verde dam experiment (26 September 2017 1730 LT, black), AHATS experiment (26 June 2008 0330 LT measured at 1.51 m above the ground, orange) and GoAmazon experiment (30 March 2014 1230 LT measured at $z/h = 1.38$, where $h = 35$ m is canopy height, blue). The corresponding IRGASON data from Rio Verde dam experiment are presented in grey. Dashed red lines correspond to the slope of the Kolmogorov law. No correction to the data is applied

6 Conclusion

Turbulence data obtained from sonic anemometers present a discrepancy between the structure function and spectrum estimates of TKE dissipation rate using the Kolmogorov theory for the inertial subrange. While aliasing creates a positive bias in estimates from the spectrum depending on how close to the Nyquist frequency the estimation is made, it does not affect structure-function estimates. Path-averaging effects, on the other hand, counter-balance part of the aliasing in spectrum estimates, while creating a negative bias in the value of ϵ estimated from the second-order structure function. The ubiquitous presence of both effects in typical atmospheric turbulence data explains the difference in those estimates observed in the literature.

Path-averaging effects, quantified here using synthetic data, can be observed in real turbulence data obtained from two separate sonic anemometers. Using transfer functions for the spectrum based on the anemometer geometry, it is possible to remove the path-averaging effect from the data, and reconstruct the inertial subrange in the second-order structure function. This correction increases the estimate of ϵ, and it was successful in recovering the inertial subrange from the 81000 Ultrasonic anemometer by Young, whereas the recovery of data from the IRGASON gas analyzer and sonic anemometer by Campbell Scientific was partial. Although a similar correction could be applied to data from the CSAT3 sonic anemometer by Campbell Scientific, in this case the second-order structure function presented an inertial subrange behaviour that does not correspond to path averaging, and for this reason the correction could not be tested.

Finally, the use of the corrected second-order structure function to estimate TKE dissipation rate is likely the best approach, as it is unbiased and presents smaller random error. This is valid for different types of sonic anemometers, as long as a transfer function derived from its geometry is available. Although the uncorrected spectrum may seem visually better due to the compensating effects of path averaging and aliasing, the level of compensation between them is not fixed, which may lead to under/overestimation of dissipation rates. In addition, the length of the inertial subrange in the structure function does not have to be as large as for spectrum, due to the fact that the structure function is an integral of the spectrum, reducing its random error.

Acknowledgements LSF was funded by the Brazilian National Council for Scientific and Technological Development (CNPq) under research Grant 401019/2017-9; NLD was also funded by CNPq under research Grants 444462/2014-7 and 303581/2013-1. We thank Fernando Armani, Rodrigo Branco Rodakoviski, Lucas Emilio B. Hoeltgebaum, André Luís Diniz dos Santos, Bianca Luhm Crivellaro and Dornelles Vissotto Junior for data collection and post processing of the Rio Verde dam experiment, and André Luiz Grion for insightful discussions.

References

Albertson JD, Parlange MB, Kiely G, Eichinger WE (1997) The average dissipation rate of turbulent kinetic energy in the neutral and unstable atmospheric surface layer. J Geophys Res Atmos 102(D12):13423–13432. https://doi.org/10.1029/96JD03346

Bendat JS, Piersol AG (2010) Random data, 4th edn. Wiley, New York

Cancelli DM, Dias NL, Chamecki M (2012) Dimensionless criteria for the production–dissipation equilibrium of scalar fluctuations and their implications for scalar similarity. Water Resour Res 48(W10522):1–14. https://doi.org/10.1029/2012WR012127

Chamecki M, Dias NL (2004) The local isotropy hypothesis and the turbulent kinetic energy dissipation rate in the atmospheric surface layer. Q J R Meteorol Soc 130(603):2733–2752. https://doi.org/10.1256/qj.03.155

Chamecki M, Dias NL, Salesky ST, Pan Y (2017) Scaling laws for the longitudinal structure function in the atmospheric surface layer. J Atmos Sci 74(4):1127–1147. https://doi.org/10.1175/JAS-D-16-0228.1

Chamecki M, Dias NL, Freire LS (2018) A TKE-based framework for studying disturbed atmospheric surface layer flows and application to vertical velocity variance over canopies. Geophys Res Lett 45(13):6734–6740. https://doi.org/10.1029/2018GL077853

Davidson P (2004) Turbulence, an Introduction for scientists and engineerers. Oxford University Press, Oxford

Davidson P, Krogstad PÅ (2014) A universal scaling for low-order structure functions in the log-law region of smoothand rough-wall boundary layers. J Fluid Mech 752:140–156. https://doi.org/10.1017/jfm.2014.286

Dias NL (2017) Smoothed spectra, ogives, and error estimates for atmospheric turbulence data. Boundary-Layer Meteorol 166(1):1–29. https://doi.org/10.1007/s10546-017-0293-7

Fairall CW, Larsen SE (1986) Inertial-dissipation methods and turbulent fluxes at the air–ocean interface. Boundary-Layer Meteorol 34(3):287–301. https://doi.org/10.1007/BF00122383

Fuentes JD, Chamecki M, dos Santos RMN, Randow CV, Stoy PC, Katul G, Fitzjarrald D, Manzi A, Gerken T, Trowbridge A, Freire LS, Ruiz-Plancarte J, Maia JMF, Tóta J, Dias N, Fisch G, Schumacher C, Acevedo O, Mercer JR (2016) Linking meteorology, turbulence, and air chemistry in the Amazon rainforest. Bull Am Meteorol Soc 97(12):2329–2342. https://doi.org/10.1175/BAMS-D-15-00152.1

Gobbi MF, Chamecki M, Dias NL (2006) Application of digital filtering for minimizing aliasing effects in atmospheric turbulent surface layer spectra. Water Resour Res 42(3):1–7. https://doi.org/10.1029/2005WR004374

Henjes K (1998) Justification of the inertial dissipation technique in anisotropic mean flow. Boundary-Layer Meteorol 88(2):161–180. https://doi.org/10.1023/A:1001138218181

Horst TW, Oncley SP (2006) Corrections to inertial-range power spectra measured by Csat3 and solent sonic anemometers, 1. Path-averaging errors. Boundary-Layer Meteorol 119(2):375–395. https://doi.org/10.1007/s10546-005-9015-7

Horst TW, Semmer SR, Maclean G (2015) Correction of a non-orthogonal, three-component sonic anemometer for flow distortion by transducer shadowing. Boundary-Layer Meteorol 155(3):371–395. https://doi.org/10.1007/s10546-015-0010-3

Hsieh CI, Katul GG (1997) Dissipation methods, Taylor's hypothesis, and stability correction functions in the atmospheric surface layer. J Geophys Res Atmos 102(D14):16391–16405. https://doi.org/10.1029/97JD00200

Jiménez j (1998) Turbulent velocity fluctuations need not be Gaussian. J Fluid Mech 376:139–147. https://doi.org/10.1017/S0022112098002432

Juneja A, Lathrop DP, Sreenivasan KR, Stolovitzky G (1994) Synthetic turbulence. Phys Rev E 49:5179–5194. https://doi.org/10.1103/PhysRevE.49.5179

Kaimal JC, Wyngaard JC, Haugen DA (1968) Deriving power spectra from a three-component sonic anemometer. J Appl Meteorol 7(5):827–837. https://doi.org/10.1175/1520-0450(1968)007%3C0827:DPSFAT%3E2.0.CO;2

Kaimal JC, Wyngaard JC, Izumi Y, Coté OR (1972) Spectral characteristics of surface-layer turbulence. Q J R Meteorol Soc 98(417):563–589. https://doi.org/10.1002/qj.49709841707

Lumley JL (1964) The spectrum of nearly inertial turbulence in a stably stratified fluid. J Atmos Sci 21(1):99–102. https://doi.org/10.1175/1520-0469(1964)021%3C0099:TSONIT%3E2.0.CO;2

Monin A, Yaglom A (1981) Statistical fluid mechanics, volume II: mechanics of turbulence, 2nd edn. MIT Press, Cambridge

Pan Y, Chamecki M (2016) A scaling law for the shear-production range of second-order structure functions. J Fluid Mech 801:459–474. https://doi.org/10.1017/jfm.2016.427

Poggi D, Katul G, Albertson J (2006) Scalar dispersion within a model canopy: measurements and three-dimensional lagrangian models. Adv Water Resour 29(2):326–335. https://doi.org/10.1016/j.advwatres.2004.12.017

Pope SB (2000) Turbulent flows. Cambridge University Press, Cambridge

Salesky ST, Chamecki M (2012) Random errors in turbulence measurements in the atmospheric surface layer: implications for Monin–Obukhov similarity theory. J Atmos Sci 69(12):3700–3714. https://doi.org/10.1175/JAS-D-12-096.1

Shinozuka M, Deodatis G (1991) Simulation of stochastic processes by spectral representation. Appl Mech Rev 44(4):191–204. https://doi.org/10.1115/1.3119501

Smalikho IN, Banakh VA, Pichugina YL, Brewer WA, Banta RM, Lundquist JK, Kelley ND (2013) Lidar investigation of atmosphere effect on a wind turbine wake. J Atmos Ocean Technol 30(11):2554–2570. https://doi.org/10.1175/JTECH-D-12-00108.1

Warhaft Z (2000) Passive scalars in turbulent flows. Annu Rev Fluid Mech 32(1):203–240. https://doi.org/10.1146/annurev.fluid.32.1.203

Webb EK (1964) Ratio of spectrum and structure-function constants in the inertial subrange. Q J R Meteorol Soc 90(385):344–346. https://doi.org/10.1002/qj.49709038520

Wilson JD (2000) Trajectory models for heavy particles in atmospheric turbulence: comparison with observations. J Appl Meteorol 39(11):1894–1912. https://doi.org/10.1175/1520-0450(2000)039%3C1894:TMFHPI%3E2.0.CO;2

Zahn E, Chor TL, Dias NL (2016) A simple methodology for quality control of micrometeorological datasets. Am J Environ Eng 6(4A):135–142. https://doi.org/10.5923/s.ajee.201601.20